An IFT20 mechanotrafficking axis is required for integrin recycling, focal adhesion dynamics, and polarized cell migration

Steven Su, Salma Begum, and Ellen J. Ezratty*
Department of Pathology and Cell Biology, College of Physicians and Surgeons, Columbia University Irving Medical Center, Columbia University, New York, NY 10032

ABSTRACT Directional cell migration drives embryonic development, cancer metastasis, and tissue repair and regeneration. Here, we examine the role of intraflagellar transport (IFT) 20 (Ift20) during polarized migration of epidermal cells. IFT20 is implicated in regulating cell migration independently of the primary cilium, but how IFT proteins integrate with the cell migration machinery is poorly understood. We show that genetic ablation of IFT20 in vitro slows keratinocyte migration during wound healing. We find that this phenotype is independent of the primary cilium and instead can be attributed to alterations in integrin-mediated mechanotransduction and focal adhesion (FA) dynamics. Loss of Ift20 resulted in smaller and less numerous FAs and reduced the levels of activated FA kinase. Studies of FA dynamics during microtubule-induced FA turnover demonstrated that Ift20 loss specifically impaired the reformation, but not the disassembly, of FAs. In the absence of Ift20 function, β1 integrins endocytosed during FA disassembly are not transferred out of Rab5 (+) endosomes. This defective transit from the early endosome disrupts eventual recycling of β1 integrins back to the cell surface, resulting in defective FA reformation. In vivo, conditional ablation of Ift20 in hair follicle stem cells (HF-SCs) similarly impairs their ability to invade and migrate during epidermal wound healing. Using explant studies, lineage tracing, and clonal analysis, we demonstrate that Ift20 is required for HF-SC migration and their contribution to epidermal regeneration. This work identifies a new Ift20 mechanotrafficking mechanism required for polarized cell migration and stem cell–driven tissue repair.

INTRODUCTION

Cell migration is vital to numerous physiological processes such as embryonic development, cancer metastasis, and tissue repair and regeneration. A variety of extracellular and intracellular factors govern the ability of a cell to propel itself in a directed manner. Extra-

cellular factors include the extracellular matrix (ECM) surrounding migrating cells as well as various chemoattractants and mechanical signals derived from the extracellular environment (Mayor and Etienne-Manneville, 2016). Intracellular components that control cell migration include dynamic actin and microtubule networks as well as protein trafficking and recycling pathways necessary to regulate the polarity and plasma membrane composition of a cell (Mayor and Etienne-Manneville, 2016). Linking the ECM to the intracellular cytoskeletal network are dynamic, integrin-based protein complexes referred to as focal adhesions (FAs). FA dynamics are essential for directional cell migration, as they are formed at sites of cell adhesion to the ECM and mediate mechanotransduction and integrin signaling (Tapial Martinez et al., 2020).

Polarized cell migration requires the dynamic assembly and disassembly of FAs. FA disassembly can be triggered by microtubule targeting of FAs (Krylyshkina et al., 2002), which induces clathrin-dependent endocytosis of FA-associated integrin (Ezratty et al., 2009).

Endocytosed integrin derived from FAs then transits through Rab5 (+) endosomal compartments and remains in an active but unliganded state in Rab11 (+) endosomes. Rab5, Rab11, Src, and PIPKIγ are required to recycle endocytosed integrin back to the plasma membrane, where it is then reassembled into FAs polarized toward the leading edge of migrating cells (Nader *et al.*, 2016).

Here we examine the role of intraflagellar transport (IFT) 20 (Ift20) in keratinocyte migration and during epidermal wound healing. Ift20 is crucial in ciliogenesis, the formation of the primary cilium of a cell (Follit *et al.*, 2006). Ift20 and other IFT proteins form complexes that traffic cargo into and out of the primary cilium of a cell (Follit *et al.*, 2006; Singla and Reiter, 2006). Loss of IFT proteins, including Ift20, can inhibit ciliogenesis both in vitro and in vivo (Follit *et al.*, 2006; Singla and Reiter, 2006). Interestingly, loss or defects in primary cilia can lead to a variety of developmental disorders such as Bardet–Beidl syndrome, Joubert syndrome, and Meckel–Gruber syndrome (Singla and Reiter, 2006; Waters and Beales, 2011). Many of the phenotypes seen in these ciliopathies are associated with defective cell migration during development (Tobin *et al.*, 2008; Waters and Beales, 2011).

In addition to ciliogenesis, Ift20 has been identified to regulate cancer cell invasiveness and collective cell migration independent of the primary cilium, through its role at the Golgi complex (Nishita *et al.*, 2017; Aoki *et al.*, 2019). Ift20 is immunolocalized to the Golgi complex in addition to the primary cilium of cells (Follit *et al.*, 2006; Nishita *et al.*, 2017; Aoki *et al.*, 2019). In nonciliated cancer cells, loss of Ift20 has been shown to fragment the Golgi complex, disrupt trafficking, and ultimately reduce cancer cell invasiveness and collective cell migration (Nishita *et al.*, 2017). Alternatively, it has been proposed that the reduced collective cell migration observed subsequent to knockdown of Ift20 is due to the inability of the Golgi complex to properly polarize due to its fragmented nature (Aoki *et al.*, 2019).

Ift20 has also been identified to regulate recycling of cell surface receptors (Finetti *et al.*, 2009, 2014). In T-cells, Ift20 regulates endosomal recycling of T-cell receptors crucial for immune synapse activation independent of primary cilia (Finetti *et al.*, 2009, 2014; Galgano *et al.*, 2017). Specifically, Ift20 works in tandem with the Rab GTPase network to ensure proper recycling of T-cell receptors at the immune synapse (Finetti *et al.*, 2009, 2014; Galgano *et al.*, 2017). Loss of Ift20 blocks recycling of T-cell receptors and results in entrapment of T-cell receptors within Rab5-positive endosomes (Finetti *et al.*, 2014).

These examples demonstrate the multifaceted roles for Ift20 within a cell: ciliogenesis, trafficking, and endosomal recycling. Interestingly, IFT88 is required for the wound healing of mouse skin (Schneider *et al.*, 2010), and embryonic knockout (KO) of various IFTs and ciliary proteins lead to developmental defects associated with underlying problems with cell motility (Veland *et al.*, 2014). Although IFT function and signaling through primary cilia have been linked to defects in cell polarity and directional migration, how IFTs integrate with the cell migration machinery to drive cell motility is poorly understood. Given the breadth of ciliopathy phenotypes that may have underlying defects in cell polarity and/or cell migration, and the general importance of cell migration, we have interrogated the function of IFT20 in vitro, during polarized migration of primary mouse keratinocytes (1°MKs), and in vivo, during epidermal wound healing.

RESULTS

IFT20 is required for polarized migration of cultured primary keratinocytes

To determine whether IFT20 is generally required for epidermal motility, we established Ift20 conditional KO (cKO) cultures of 1°MKs

and examined them for defects in cell migration (see *Materials and Methods*). IFT20 fl/fl Rosa-tdTomato reporter basal stem cells were isolated from mouse epidermis and transduced with a lentiviral (LV) Cre to establish Ift20 cKO keratinocyte cell lines (Figure 1A). Transduction with LV-Cre induced bright Tomato reporter fluorescence, an indication of Cre-recombinase activity and likely floxing out of the IFT20 allele (Figure 1B). Immunofluorescence (IF) of Ift20, which colocalized to the Golgi apparatus (Follit *et al.*, 2006) was reduced in Tomato(+) keratinocytes in comparison to neighboring, nontransduced cells (Figure 1B, arrowheads). Ift20 protein was quantitatively reduced in keratinocyte cultures transduced with LV-Cre, in comparison to nontransduced cell lines (Figure 1C). Ift20 cKO and control keratinocytes were subjected to an in vitro scratch wound and monitored for 18 h to determine the rate of wound closure. Ift20 cKO primary mouse keratinocytes showed markedly delayed cell migration toward an in vitro wound (Figure 1, D, and E). We conclude that Ift20 plays an essential function during the polarized migration of keratinocytes in response to in vitro wound repair.

Ablation of IFT20 does not affect Golgi polarization or overall structure in cultured keratinocytes

Previous studies of Ift20 function during cell migration have implicated it in regulating Golgi polarization (Nishita *et al.*, 2017; Aoki *et al.*, 2019). We hypothesized that the cell migration defects in IFT20 null keratinocytes could similarly be due to defects in the Golgi apparatus. However, in cultured keratinocytes stimulated to migrate into an in vitro wound, polarization of the Golgi apparatus toward the leading edge is not robustly detected even under control conditions, and cKO of IFT20 does not result in any statistically significant differences in Golgi polarization in comparison to WT controls (Supplemental Figure 1, A–C). Ift20 has also been implicated in maintaining the structure of the Golgi, and cancer cells depleted of IFT20 via short hairpin RNA display a fractured and disorganized Golgi (Nishita *et al.*, 2017). Quantification of Golgi fragment area per cell showed that the cKO of IFT20 did not significantly affect overall Golgi structure/fragmentation in comparison to control keratinocytes (Supplemental Figure 1, D and E). Taken together, these results suggest that Ift20 is not required for Golgi polarization or the maintenance of Golgi structure in 1°MKs.

Loss of IFT20 leads to defects in mechanochemical signal transduction that is independent of the primary cilium

To understand the IFT20-dependent mechanism that is required for optimal cell migration, we sought to determine whether there is an essential mechano- or chemosensory function of IFT20/cilia required for keratinocyte motility. Previous studies have shown that primary cilia orient toward the wound edge of migrating fibroblasts (Christensen *et al.*, 2013). It has been hypothesized that cilia may sense extracellular cues that determine the speed or directionality of cell migration (Schneider *et al.*, 2010). We analyzed ciliogenesis in 1°MKs that have been stimulated to migrate toward an in vitro scratch wound, but <2% of these cells displayed primary cilium under growth conditions that are optimal for cell motility (Supplemental Figure 2; also see Ezratty *et al.*, 2011). These data suggest that Ift20 plays an extraciliary role during polarized migration of 1°MKs.

Polarized cell migration requires activation of integrin-mediated cell adhesion, which is translated to changes in the phosphorylation status of mechanically sensitive proteins (Tapial Martinez *et al.*, 2020). FA kinase, or FAK, is an adhesion-activated scaffolding protein that resides at sites of activated integrin signaling, the FA (Burridge, 2017). Autophosphorylation of FAK at Y397 is a sensitive readout of mechanotransduction via integrin-mediated adhesion
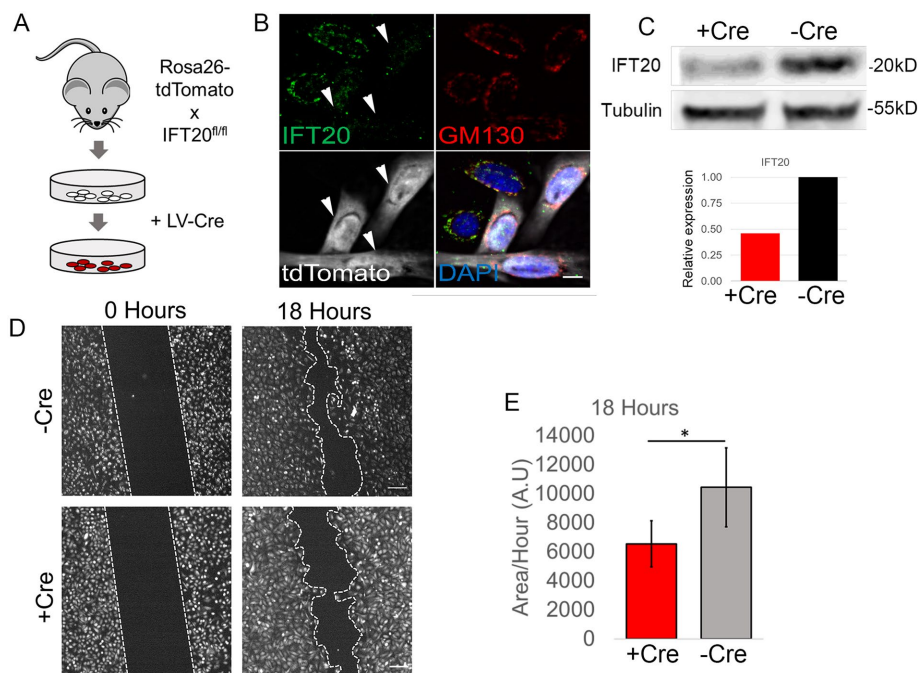
FIGURE 1: IFT20 is required for the polarized migration of primary keratinocytes in response to in vitro wound repair. (A) Schematic of keratinocyte isolation from IFT20 fl/fl Rosa 26-tdTomato skin and transduction of lentiviral-Cre (LV-Cre), which induced Tomato fluorescence. (B) IF images of Ift20 and GM130 in IFT20 fl/fl Rosa-Tomato keratinocytes. Arrowheads point to Cre-transduced Tomato (+) cells that show reduction in Ift20 immunolabeling. DAPI marks nucleus. Scale bar indicates 10 μm. (C) Western blot of IFT20 protein from control (–Cre) or Cre-transduced (+Cre) keratinocytes. Tubulin is loading control. Histogram is quantification of bands shown above. (D) IFT20 fl/fl –Cre (control) or + Cre (Cre-transduced) keratinocytes were subject to scratch assay, and migration was monitored for 18 h. Dotted line indicates wound edge. Scale bar indicates 150 μm. (E) Quantification of migration rate in +Cre or –Cre IFT20 fl/fl cells. Data in histogram represent $n = 5$ independent experiments where the area of wound closure was measured after 18 h of cell migration. * indicates $p = 0.03$ by Student's t test. Error bars indicate SD. A.U. indicates arbitrary units.

signaling (Zhao and Guan, 2011). Interestingly, protein lysates from IFT20 cKO keratinocytes show reduced phosphorylation of Y397 FAK, indicating a possible defect in adhesion-mediated FAK activation (Figure 2, A and B). To determine whether there are any defects in cell adhesion, Ift20 cKO keratinocytes were stained with vinculin, a resident FA protein. By IF, FAs appeared smaller and less numerous in IFT20 cKO cells in comparison with control keratinocytes (Figure 2C). Quantification of total FA area per cell demonstrated a two- to threefold decrease in the absence of IFT20 (Figure 2D). FAs were also quantitatively smaller, as the average FA area/cell was significantly reduced in IFT20 cKO keratinocytes in comparison with wild-type (WT), nontransduced control cells (Figure 2E). The difference in average FA size cannot be attributed to a difference in cellular area; cellular area remained unchanged between Cre(-) and Cre(+) IFT20 cKO keratinocytes (Figure 2F). Taken together, these results suggest that the cell migration defects we observed could be a consequence of defective integrin-mediated mechanotransduction at sites of cell–substrate contact, the FA.

IFT20 is required for FA reformation after microtubule-induced FA disassembly

Since Ift20 is a microtubule-associated protein (Absalon *et al.*, 2008), we hypothesized that it may be required for FA disassembly induced by microtubule targeting. To test this hypothesis, a nocodazole (NZ)

washout assay to study microtubule (MT)-induced FA turnover was performed in IFT20 cKO versus control keratinocytes (Ezratty *et al.*, 2005). In this experiment, keratinocytes are treated with 10 μM NZ for 3–4 h to completely depolymerize the microtubule (MT) cytoskeleton and induce Rho-dependent activation of contractility and subsequent FA formation. This is followed by a washout of NZ that induces MT polymerization, regrowth, and targeting to FAs to induce their disassembly. After 3–4 h treatment with NZ, both WT and Ift20 cKO keratinocytes formed FAs, ascertained by immunolabeling for vinculin (Figure 3A, 0 min time point). Consistent with reduced pFAK phosphorylation on Y397, IFT20 cKO keratinocytes treated with NZ displayed FAs that were slightly less numerous and smaller in size than those observed in WT cells (Figure 3, B and C). However, a time course of NZ washout showed that FAs from Ift20 cKO cells still disassembled after 15–30 min of MT regrowth during recovery from NZ (Figure 3B). We note that this time course of FA disassembly is slightly faster than what we observed in NIH3T3 fibroblasts and likely a consequence of reduced serum starvation conditions (see *Materials and Methods* and Ezratty *et al.*, 2005). The overall structure and organization of MTs appeared normal in IFT20 cKOs interphase cells that were not treated with NZ (Figure 2C). MT regrowth to the periphery of the cell membrane was still observed in the absence of Ift20 function (time course; Figure 3D), and MTs still targeted toward FAs in the absence of IFT20 (Figure 3E). These observations suggest that MT-induced FA disassembly does not require Ift20.

Next, we evaluated the effect of IFT20 cKO at further time points after MT recovery post-NZ treatment, when FAs reform via a process that requires integrin recycling (Nader *et al.*, 2016). After 60–90 min of MT regrowth, FAs in WT primary keratinocytes gradually reform toward the cell periphery (Figure 3A, quantified in B and C), a phenomenon that has been extensively studied in fibroblasts and reported in other epithelial cell types (Nader *et al.*, 2016). However, FAs from IFT20 cKO cells fail to reform with the same kinetics, and both the number and size of FAs remain significantly reduced after 90 min of MT regrowth in the IFT20 cKO cells in comparison with WT control cells (Figure 3A, quantified in B and C). These data suggest that Ift20 is required for FA reformation after MT-induced FA disassembly.

Integrin surface expression is altered when IFT20 function is ablated

Our previous studies have shown that FA reformation after MT-induced FA disassembly is driven by integrin recycling to the plasma membrane. This process requires FAK, PIPKIγ, and the Rab5/Rab11 endosomal system (Nader *et al.*, 2016). We sought to determine whether integrin trafficking or recycling is perturbed in the absence of Ift20, specifically whether FA-associated β1 integrin is properly recycled back to the plasma membrane. First, we determined whether β1
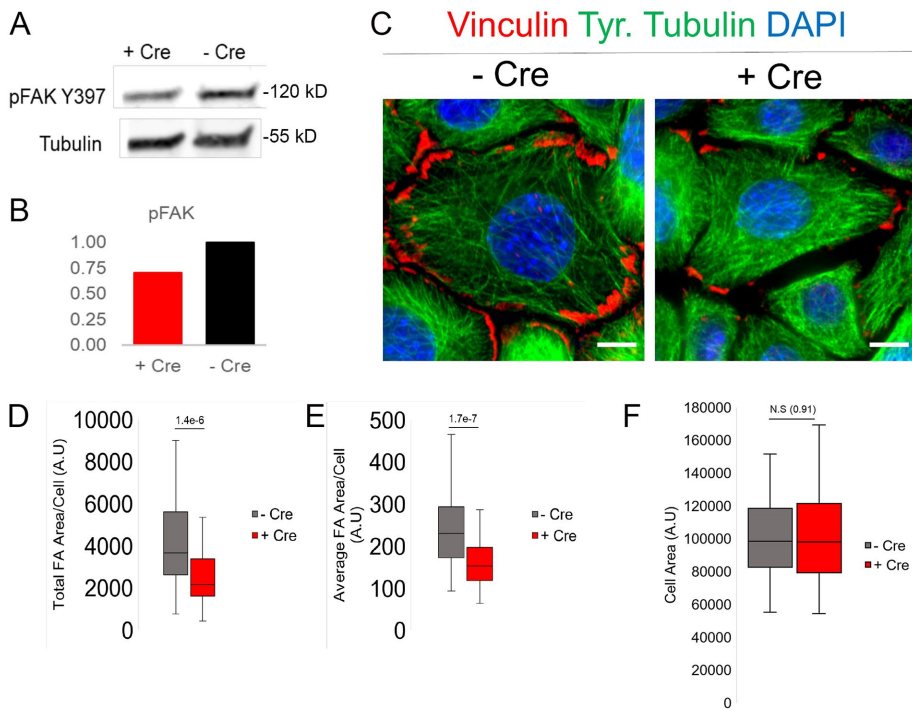
FIGURE 2: IFT20 loss results in defective mechanochemical signaling downstream of integrin engagement. (A) Western blot of pFAK Y397 protein levels from –Cre control vs. +Cre IFT20 fl/fl keratinocyte lysate. Tubulin shown as loading control. (B) Quantification of pFAK Y397 signal from bands shown in A. C) Immunolabeling for vinculin, tyrosinated tubulin, and nuclei (DAPI) in +Cre vs. –Cre IFT20 fl/fl keratinocytes. Scale bar indicates 10 μm. (D, E) Quantification of the total FA area/cell or average FA area/cell in IFT20 fl/fl keratinocytes. Histograms represent data from two independent experiments where FA size was measured in 50 or more cells in each condition. Statistical values were computed using a Mann–Whitney U test. (F) Quantification of total cell area in both –Cre and +Cre keratinocytes. Statistical value was computed using a Mann–Whitney U test.

ciliary components toward the basal body (Follit *et al.*, 2006). In nonciliated T-cells, Ift20 is also required for Rab5 and Rab11-dependent recycling of T-cell receptors to the immunological synapse independent of primary cilia (Finetti *et al.*, 2009, 2014; Galgano *et al.*, 2017). Interestingly, integrin trafficking after MT-induced FA disassembly requires Rab5/Rab11-dependent transit through the endosomal system (Nader *et al.*, 2016). A Golgi-retromer–dependent pathway of integrin recycling has also recently been identified, although the reliance of this pathway on MTs is less clear (Chen *et al.*, 2019). To decipher a role for Ift20 function via Rab5/Rab11-dependent versus Golgi/retromer trafficking mechanism(s), we began by determining the localization of Ift20 in cultured keratinocytes during MT-induced FA disassembly and polarized FA reformation. As previously reported, Ift20 localizes to the primary cilia (Supplemental Figure 3) and the Golgi apparatus (Figure 1B; Supplemental Figure 1D) in cultured primary keratinocytes (Follit *et al.*, 2006). During MT-induced FA disassembly and reformation, the Golgi is dispersed upon MT-depolymerization and reorganized upon NZ washout and MT regrowth after recovery from NZ (Figure 5A). For the duration of the NZ washout and MT regrowth, Ift20 maintains colocalization with GM130 (a marker of the Golgi apparatus) (Figure 5A). In IFT20 cKO keratinocytes, Golgi dispersion upon NZ treatment and reassembly during MT recovery both appear to be unaffected (Figure 5B). We conclude that Ift20 maintains its association with the Golgi apparatus during MT-induced FA disassembly and reformation.

integrin could be detected within the FAs of cultured 1°MKs. IF of β1 integrin shows convincing colocalization with vinculin, a resident FA-associated protein, in both untreated and NZ-incubated primary mouse keratinocytes (Figure 4A). Induction of MT-induced FA disassembly and FA reformation showed that the return of FA-associated β1 integrin is impaired when IFT20 is removed (Figure 4, B and C, 90 min time point). Next, we used the same antibody for fluorescently activated cell sorting (FACS) analysis of β1 integrin surface levels during FA disassembly and reformation during the NZ washout assay. As shown in cultured fibroblasts (Nader *et al.*, 2016), surface levels of β1 integrin decrease after 30 min of MT regrowth to induce FA disassembly (Figure 4D). After 90–120 min of MT regrowth and FA reformation, β1 surface integrin levels increase significantly in control cells (Figure 4D). These data are consistent with that shown in fibroblasts: surface integrin is removed from FAs via endocytosis during MT regrowth and recycled back to the plasma membrane into newly forming peripheral FAs (Nader *et al.*, 2016, and Figure 4D). Upon IFT20 cKO, integrin surface levels decrease at 30 min but do not return to the same extent as control cells after 90 min of MT regrowth (Figure 4D). These results strongly suggest that Ift20 is required for the polarized recycling of FA-associated β1 integrin back to the cell surface.

IFT20 maintains its association with the Golgi apparatus during FA reformation after MT-induced FA disassembly

In addition to its essential role in ciliogenesis, Ift20 functions at the Golgi apparatus, where it contributes to the polarized trafficking of

IFT20-dependent FA reformation does not require Golgi function

Our previous studies using NIH3T3 fibroblasts have shown that FA disassembly and reformation induced by MT regrowth after NZ washout does not require trafficking from the Golgi apparatus (Nader *et al.*, 2016). Given Ift20's known function(s) at the Golgi, as well as its localization at the Golgi during MT regrowth and FA disassembly/reformation, we questioned whether the Ift20-dependent process of integrin recycling to promote FA reformation might proceed via a different, Golgi-dependent mechanism in our 1°MKs such as the previously reported Retromer pathway (Chen *et al.*, 2019). To test the Golgi dependence of Ift20 in regulating mechanotransduction at FAs, we treated keratinocytes with brefeldin A (BFA) for 3 h to disrupt Golgi structure and function. As expected, treatment with BFA fragmented the Golgi in comparison to controls (Figure 5C), and Ift20 maintained its association with the disrupted Golgi fragments as previously reported (Figure 5C and Follit *et al.*, 2006). To test the Golgi dependence of Ift20 in regulating FA disassembly and reformation, 1°MKs were incubated for 3 h with BFA and NZ prior to washing out the NZ and inducing FA disassembly and reformation in the presence of BFA. Neither FA disassembly nor FA reformation after MT regrowth was affected by BFA treatment in 1°MKs (Figure 5, D and E). We conclude that the Ift20-dependent
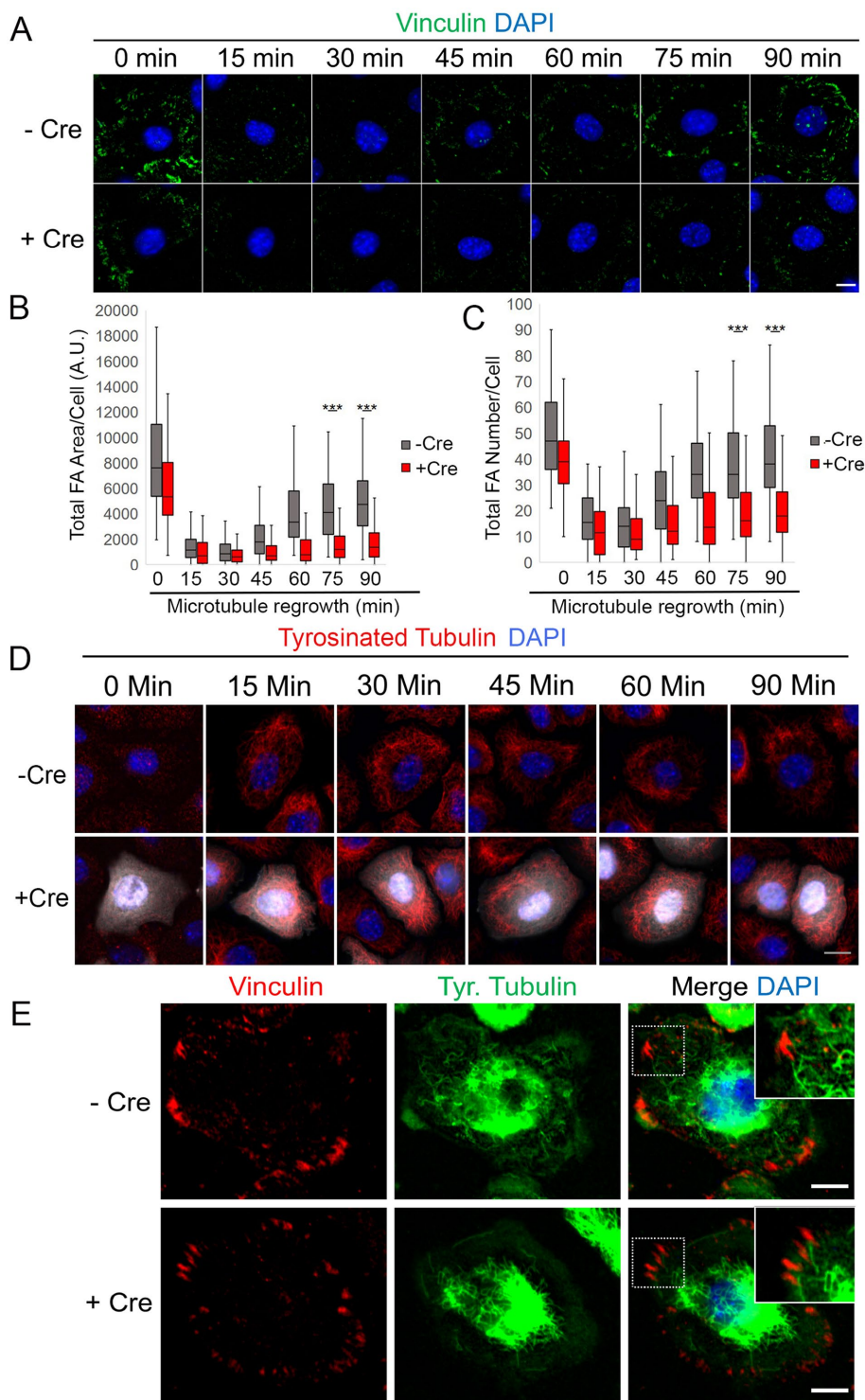
FIGURE 3: IFT20 is required for FA reformation after NZ washout and microtubule regrowth. (A) IF images of vinculin during time course of NZ washout and microtubule regrowth (min indicates minutes) in –Cre control vs. +Cre IFT20 fl/fl keratinocytes. DAPI marks nuclei. (B, C) Quantification of total FA area/cell and total FA number/cell during time course of microtubule regrowth in –Cre control vs. +Cre IFT20 fl/fl keratinocytes. Data in histograms represent $n = 3$ independent experiments where 63–127 cells were measured at each time point and each condition. *** indicates $p < 5.5e-15$ via Mann–Whitney U Test. (D) IF images of tyrosinated tubulin during time course of NZ washout and microtubule regrowth (min indicates minutes) in –Cre control vs. +Cre IFT20 fl/fl keratinocytes. DAPI marks nuclei. White indicates +Cre Tomato signal. Note that MT regrowth occurs normally and toward the periphery in +Cre cells. (E) IF images of –Cre control and +Cre IFT20 fl/fl keratinocytes 5 min after NZ washout. Note that microtubules target FAs during the FA disassembly process. Scale bars in both A and E denote 10 μm. Scale bar in D denotes 15 μm.

defects in integrin trafficking and mechanotransduction at FAs (as measured using the FA turnover assay) are independent of its localization and function at the Golgi.

IFT20 is required to traffic β1 integrin through Rab5 endosomes

We next sought to determine whether Ift20 functioned in tandem with the Rab5 endosomal system to traffic β1 integrin during FA turnover. We focused our analysis at 0, 30, and 90 min of MT regrowth following NZ washout as the 30- and 90-min time points represent time points of maximal FA disassembly and maximal FA reformation, respectively (Figure 3, A–C). At 30 min of MT regrowth, we observe increased colocalization of Ift20 with Rab5 compared with 0 min in control keratinocytes (Figure 6, A and B). In particular, at the 30-min time point, we can observe distinct puncta of Ift20 colocalizing with what appear to be small Rab5 (+) endosomal puncta (Figure 6, A and B). Following 90 min of MT regrowth, we observe sustained colocalization of Ift20 with Rab5; however, the colocalization at 90 min occurs predominantly at larger Rab5 (+) compartments instead of the smaller Rab5 (+) endosomal puncta we observe at 30 min (Figure 6, A and B). Quantification of Ift20 and Rab5 colocalization during this time course confirms our observations, mainly that colocalization of Ift20 with Rab5 increases at 30 min of MT regrowth and that this increase is sustained through 90 min of MT regrowth (Figure 6C). We next determined the fraction of β1 integrin within Rab5 (+) endosomes by calculating the colocalization coefficient of Rab5 and β1 integrin staining at 0, 30, and 90 min of MT regrowth. As previously reported, in control cells, β1 integrin colocalizes with peripheral Rab5 puncta after 30 min of MT regrowth during recovery from NZ treatment, and we observe a significant increase in the colocalization coefficient compared with 0 min (Figure 6, D–F) (Nader et al., 2016). In control cells, after 90 min of MT regrowth and FA reformation, fewer Rab5 (+) endosomes containing integrin are detected and the colocalization coefficient significantly decreases compared with the 30-min time point (Figure 6,E and F). In IFT20 fl//fl 1°MKs transduced with Cre to ablate Ift20 function, we observe a significant increase of β1 integrin colocalizing with peripheral Rab5 puncta at the 30-min time point, but importantly there is no significant decrease in colocalization between β1 integrin and Rab5 puncta at the 90-min time point (Figure 6, E and F). In fact there is a statistically significant increase in the amount of internalized β1 integrin colocalizing with
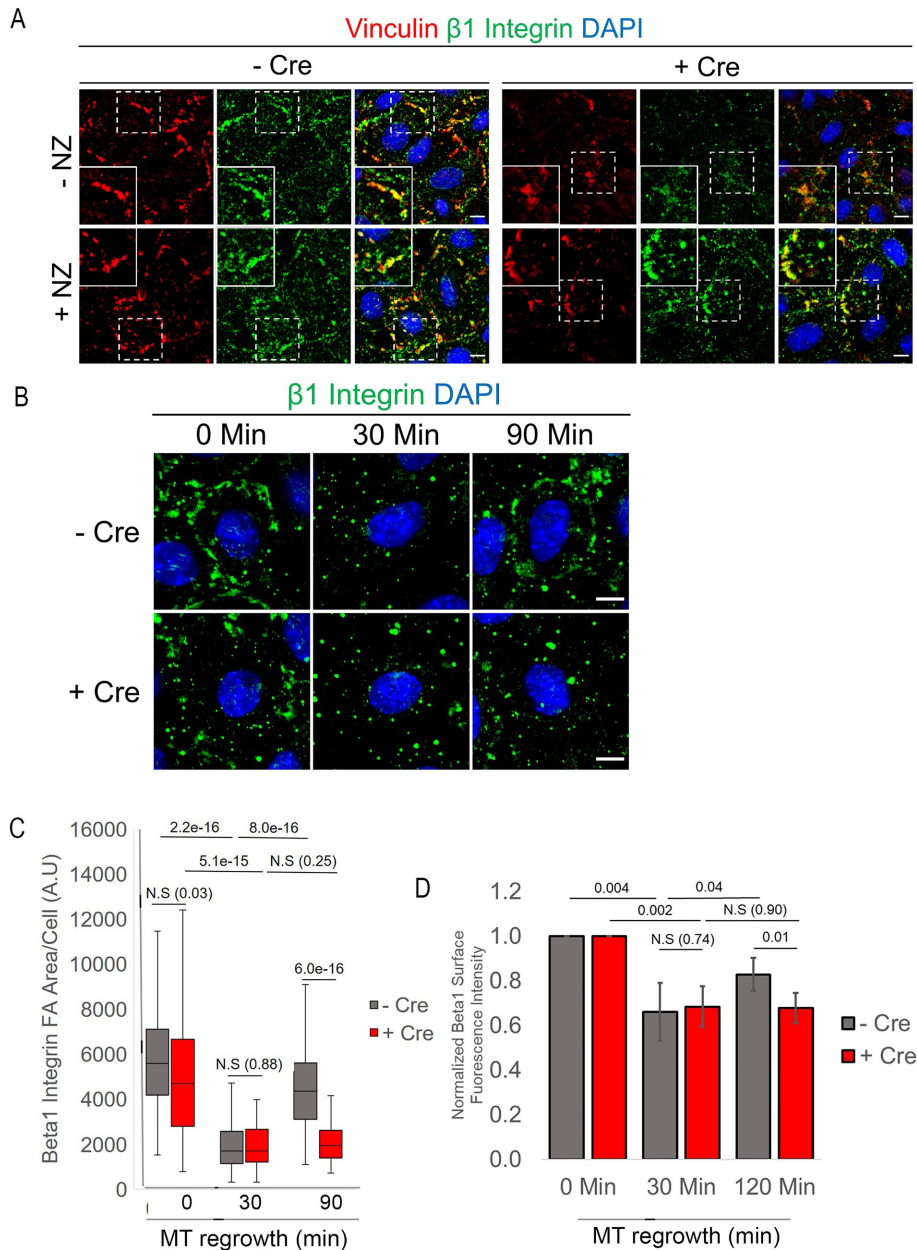
A Vinculin β1 Integrin DAPI

- Cre   + Cre

- NZ

+ NZ

B β1 Integrin DAPI

0 Min   30 Min   90 Min

- Cre

+ Cre

C

Beta1 Integrin FA Area/Cell (A.U)

2.2e-16   8.0e-16
5.1e-15   N.S (0.25)
N.S (0.03)
N.S (0.88)
6.0e-16

- Cre
+ Cre

MT regrowth (min)

D

Normalized Beta1 Surface Fluorescence Intensity

0.004   0.04
0.002   N.S (0.90)
N.S (0.74)   0.01

0 Min   30 Min   120 Min

- Cre
+ Cre

MT regrowth (min)

FIGURE 4: Surface levels of recycled β1 integrin, previously present in FAs, are decreased upon IFT20 knockout. (A) IF images of vinculin (red) and β1 integrin (green) in –Cre control vs. +Cre IFT20 fl/fl keratinocytes treated with NZ for 3–4 h or left untreated. Boxed regions are shown magnified in the corner. Merged image with DAPI (nuclei) shows colocalization of β1 integrin and vinculin IF signals. Scale bars indicate 10 μm. (B) Representative images of β1 integrin IF at various time points following NZ washout (min indicates minutes). DAPI indicates nuclei. Scale bar indicates 10 μm. (C) Quantification of β1 integrin IF at FAs at various time points following NZ washout (min) in –Cre control and +Cre IFT20 fl/fl keratinocytes. Data in histogram represent $n = 60–81$ cells per time point/per condition from two independent experiments. Statistical values were computed using a Mann–Whitney U test. (D) Normalized flow cytometry measurements of surface β1 integrin following NZ washout. Data are from $n = 5$ independent experiments with more than 5000 cells measured per condition at each time point. Error bars indicate SD. Statistical values were computed using a Student's t test.

Rab5 after 90 min in IFT20 cKO cells compared with control (Figure 6E). Taken together, because we observe an increased colocalization of Rab5 (+) endosomes with Ift20 and Rab5 (+) endosomes with β1 integrin after 30 min of MT regrowth, these data suggest that Ift20 is required for the transit of β1 integrin out of Rab5 (+) endosomes. Our

in vitro data are consistent with the following model: in the absence of Ift20 function, integrin that has been endocytosed from disassembling FAs is not transferred from Rab5 (+) endosomes and fails to be recycled back to the cell surface. This defective trafficking deleterously affects FA turnover, mechanotransduction, and overall cell migration efficiency.

IFT20 is required for the in vivo mobilization of epidermal stem cells in response to epidermal injury

Ift20 function has previously been implicated in regulating the cell invasiveness of colon cancer cell lines in vitro (Nishita *et al.*, 2017; Aoki *et al.*, 2019). To study Ift20 function during cellular invasion and migration in a physiologically relevant model system, we turned to the tissue-resident stem cells of the epidermal hair follicle. Hair follicle stem cells (HF-SCs) transiently contribute to tissue regeneration during epidermal repair, when they are activated to leave their niche, invade the surrounding tissue, and migrate toward the wounded epidermis (Ito *et al.*, 2005; Ito and Cotsarelis, 2008). To efficiently invade and migrate, HF-SCs must sense mechanochemical changes from the wound microenvironment and transduce these cues to the cell's migration machinery (Fuchs, 2016). Given our in vitro migration data, we hypothesized that Ift20 may play a conserved role in polarized migration and invasion of HF-SCs in vivo.

To study the function of IFT20 exclusively in HF-SCs, we generated an inducible cKO mouse model where IFT20 could be specifically ablated in the HF-SC "bulge" compartment (Bose *et al.*, 2013). In particular, we mated K15-Cre[PGR] mice to IFT20 fl/fl mice (Jonassen *et al.*, 2008). K15-Cre drives recombination specifically in HF-SCs, and these mice were maintained on a Rosa26-Tomato reporter background to monitor Cre activation and for lineage tracing (Figure 7A). Telogen-staged mice were treated topically with 1% RU-486 to induce K15-Cre–mediated recombination specifically in HF-SCs (Figure 7B), which induced a strong Rosa-Tomato signal in 80–90% of HFs (Figure 7C). The Ift20 signal was uniformly reduced in Tomato (+) IFT20 cKO HF-SCs, but not cells of the interfollicular epidermis (IFE), indicating that K15-Cre–mediated floxing of IFT20 occurred specifically in the bulge stem cell compartment (Figure 7D). High-magnification imaging of telogen-staged mouse skin reveals that Ift20 is perinuclear in its localization within keratinocytes of the HF (Supplemental Figure 4). Ciliogenesis was quantitatively inhibited, as expected, in the Rosa (+) HF-SCs (Figure 7E). Quantitative PCR (qPCR) from FACS-isolated HF-SCs demonstrated a significant
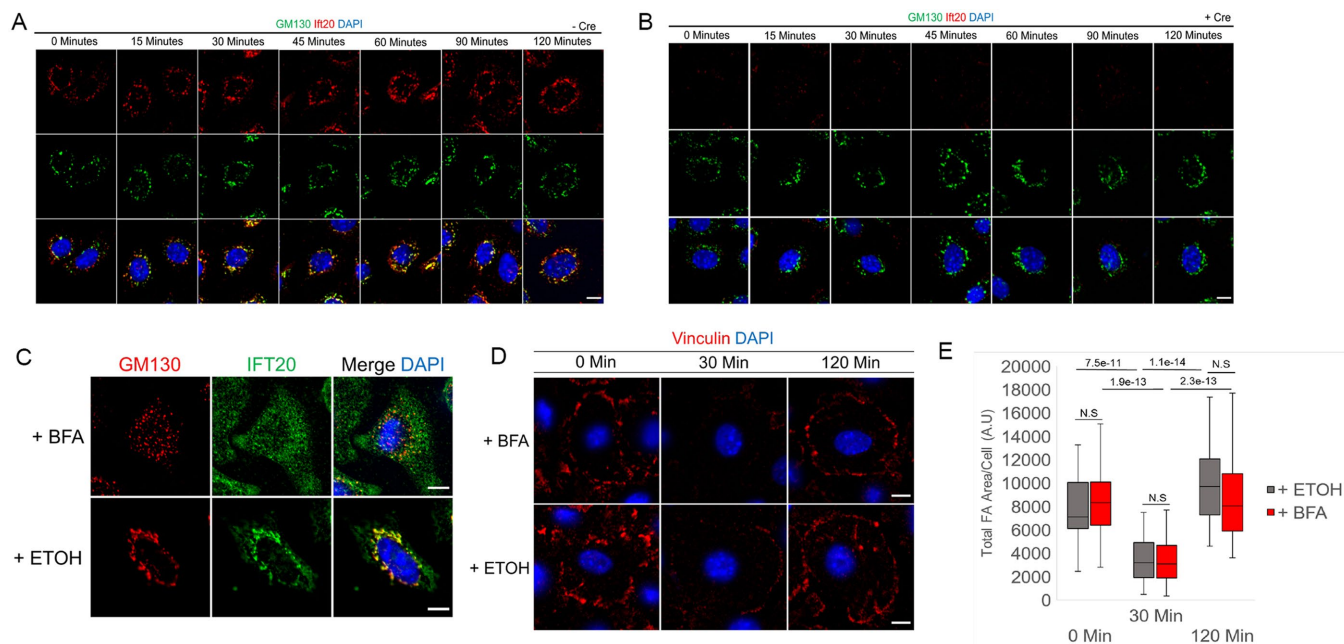
FIGURE 5: IFT20-dependent FA reformation is independent of its localization or function at the Golgi. (A, B) IF images of GM130 and Ift20 with DAPI marking nuclei of –Cre control (A) and +Cre (B) IFT20fl/fl keratinocytes during microtubule-induced FA disassembly and reformation at various time points after NZ washout (shown in minutes). Scale bars indicate 10 μm. (C) IF images of GM130 and Ift20 in control keratinocytes treated with brefeldin A (BFA) or loading control (ETOH) for 3 h. DAPI marks nuclei. Scale bar indicates 10 μm. (D) IF images of vinculin in control keratinocytes during various time points following NZ washout in the presence of BFA or loading control (ETOH) after prior pretreatment with BFA or ETOH. DAPI indicates nuclei. Scale bars indicate 10 μm. (E) Quantification of total FA area/cell in control keratinocytes during time course following NZ washout in the presence of BFA or loading control (ETOH) after prior pretreatment of cells with BFA or ETOH. Data obtained from $n = 40$ cells per time point per condition from two independent experiments. Statistical values were computed using a Mann–Whitney U test.

reduction in IFT20 expression (Figure 7, F and G). These data show that IFT20 expression and ciliogenesis can be conditionally ablated specifically in HF-SCs.

To test whether Ift20 is required for HF-SC migration in response to epidermal injury, K15-Cre IFT20 cKO mice were subject to a full-thickness epidermal punch biopsy, and lineage tracing was used to measure the mobilization of cKO HF-SCs to the epidermis after 4 or 7 d of wound healing (Figure 7, H and I, and Supplemental Figure 5). In IFT20+/fl (essentially WT) mice, Tomato (+) cells were observed both in the wound-adjacent epidermis and in the wound bed, where they proliferated into epidermal clones (Figure 7, H and I). In contrast, Ift20 cKO Tomato (+) cells were more rarely detected in the epidermis and significantly reduced in the wound bed (Figure 7, H and I). Quantitative analysis demonstrated that loss of Ift20 impaired the mobilization of Tomato (+) HF-SCs to the injured epidermis after 4 d of wound healing (Figure 7K). Similar results are observed at 7 d of wound healing although with greater variation (Supplemental Figure 5). These data suggest that IFT20 is required for the transient mobilization of HF-SCs to the epidermis and their clonal contribution to epidermal repair.

IFT20 is required for stem cell migration from skin explants taken from wound biopsies

To test whether Ift20 is required for polarized cell migration of HF-SCs from skin explants, IFT20 cKO/Rosa-Tomato explants and IFT20 +/fl/Rosa-Tomato ("WT") controls were grown from biopsied mouse skin isolated from in vivo wound healing studies. After 14 d of culture, IFT20 +/fl Tomato (+) HF-SCs migrated out of the bulge cell niche to the surface of the epithelial explant, whereas IFT20 cKO

Tomato (+) HF-SCs are rarely observed migrating to the surface under these ex vivo conditions (Figure 7L). These data demonstrate that Ift20 is required to mobilize SCs from their HF niche during injury repair and suggest that Ift20-dependent trafficking of adhesion receptors may modulate the regenerative response and invasion of HF-SCs toward epidermal injury.

DISCUSSION

Polarized cell migration is essential for embryonic patterning and development, drives tissue regeneration in response to wound repair, and contributes to numerous pathological conditions. Human ciliopathies, which are caused by a wide variety of defects in the primary cilium, display features associated with disrupted cell migration (Spasic and Jacobs, 2017). Defects in the formation or function of primary cilia can lead to migration-related disorders in mice, such as defects in skin wound healing and repair of the corneal epithelium (Veland et al., 2014). However, whether defects in directional cell migration are a direct function of defective signaling through the primary cilium remains unclear.

To efficiently invade and migrate, epithelial cells must sense mechanochemical changes from the wound microenvironment and transduce these cues to the cell's migration machinery. The primary cilium is a microtubule-based cellular "antenna" that can detect mechanical and chemical changes in the extracellular environment; and many of the signaling pathways that require primary cilia for their transduction (Shh, Notch, Wnt) are also essential for cell migration (Goetz and Anderson, 2010). Previous studies have shown that primary cilia orient toward the wound edge during polarized cell migration of cultured fibroblasts (Christensen et al., 2013), suggesting
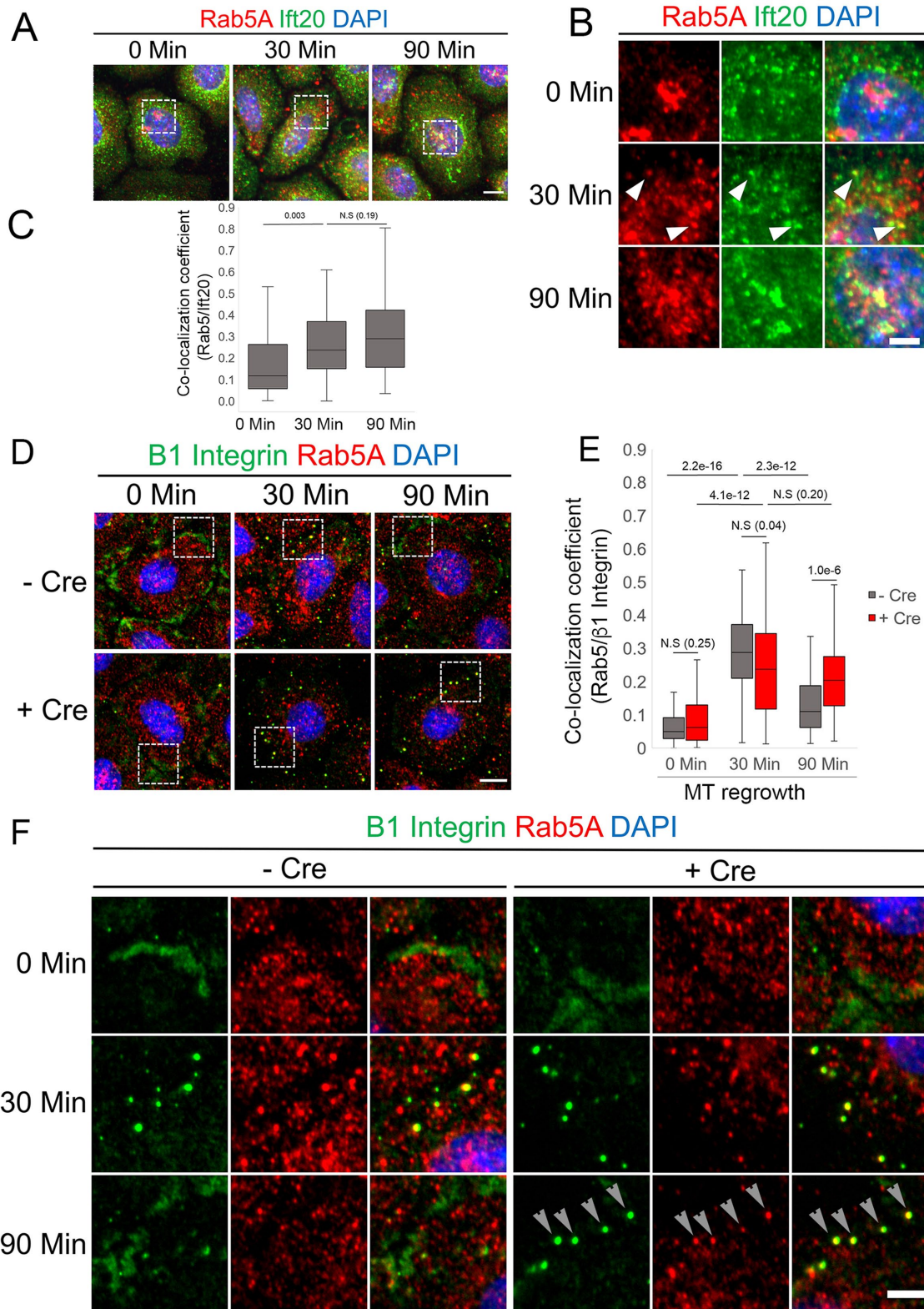
FIGURE 6: Ift20 is required to transit β1 integrin through Rab5(+) endosomes during MT-induced FA turnover. (A) IF images of Ift20 and Rab5A at indicated time points following NZ washout. Scale bar indicates 10 μm, and min indicates minutes. Boxed regions are magnified in B). (B) Magnified images of boxed regions shown in A). Scale bar indicates 5 μm, and min indicates minutes. Arrowheads indicate distinct puncta showing colocalization of Rab5 and Ift20. (C) Quantification of colocalization of Rab5 and Ift20 as measured by a colocalization coefficient. Statistical values were computed using a Mann–Whitney U test. Data represent more than 60 cells per condition obtained from two independent experiments. (D) IF micrographs of −Cre control or +Cre IFT20 fl/fl keratinocytes at various time points during FA turnover (min indicates minutes) showing the localization of β1 integrin and Rab5 endosomal
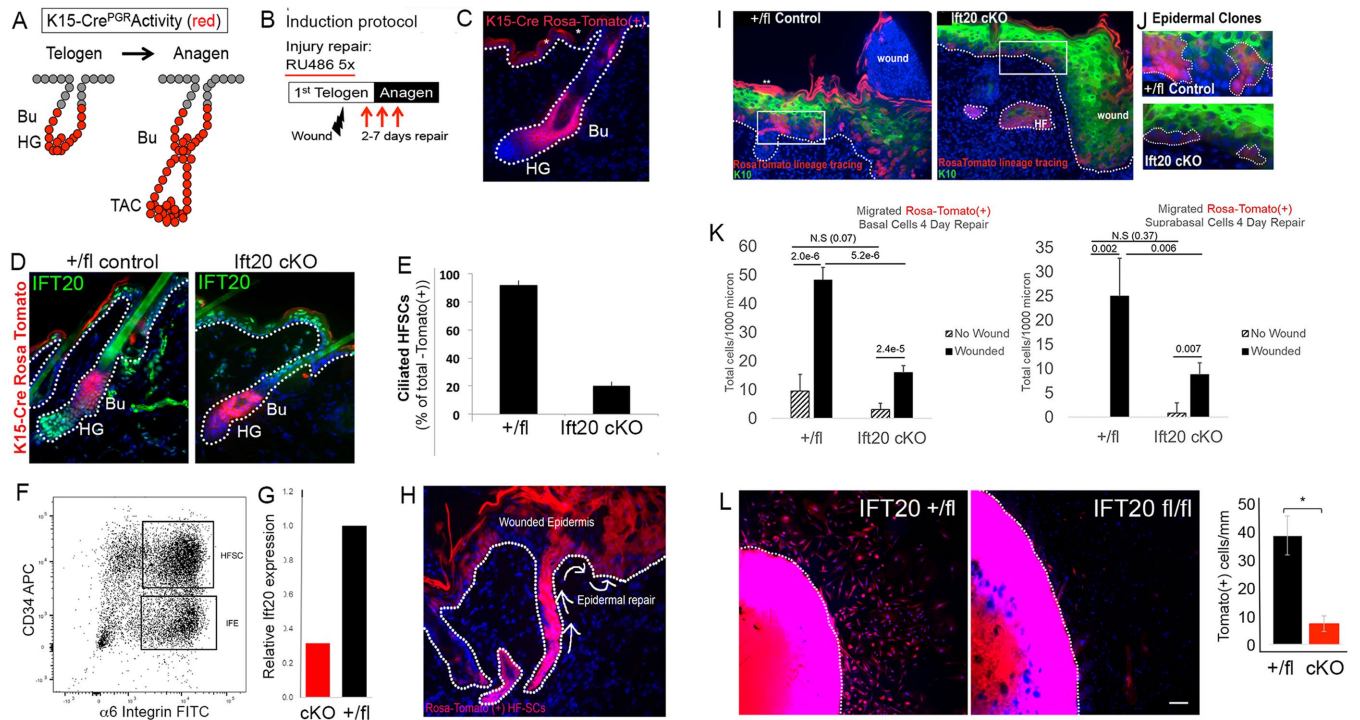
FIGURE 7: IFT20 is required for the polarized migration and invasion of hair follicle–derived stem cells and their clonal contribution to wound repair. (A) Schematic of lineage tracing strategy showing the localization of K15-Cre Tomato(+) HF-SCs. (B) Schematic of strategy used for RU486 treatment and Cre induction prior to wound healing and epithelial repair (see *Materials and Methods*). (C) IF images of Tomato(+) signal (red) labeling the HF-SCs of the bulge (Bu) and their transiently amplifying progenitors in the hair germ (HG). (D) IF images of Ift20 in HF-SCs (red) of control (IFT20 +/fl) vs. IFT20 cKO (IFT20 fl/fl) telogen staged mouse skin. (E) Quantification of the number of ciliated HF-SCs in control (IFT20 +/fl) vs. IFT20 cKO (IFT20 fl/fl) skin. Data in histogram represent 20–30 hair follicles from *n* = 3 mice. (F) Scatter plot from FACS purification of CD34 (high)/α6 integrin (high)/Tomato (+) HF-SCs. (G) qPCR of IFT20 using mRNA isolated from FACS-purified HF-SCs from WT (IFT20 +/fl) vs. IFT20 cKO (IFT20 fl/fl) mouse skin. (H) Sagittal section of skin isolated from WT control (IFT20 +/fl) Rosa Tomato(+) mouse subjected to a full-thickness punch biopsy wound. IF image shows HF-SCs (red) migrating toward, and contributing to, the epidermal wound bed. Arrows indicate direction of migration, dotted line denotes dermal–epidermal border, and DAPI (blue) label nuclei. (I) Sagittal sections from control (IFT20 +/fl) or IFT20 cKO (IFT20 fl/fl) wounded epidermis demonstrating migrated HF-SCs (red), keratin 10 (K10) to label suprabasal layer (green), and DAPI-labeled nuclei. Boxed region is magnified at right in (J). (J) Examples of epidermal clones from control vs. IFT20 cKO epidermis. (K) Quantification of the number of migrated Rosa-Tomato (+) HF-SCs and their contribution to basal or suprabasal layers of the wounded epidermis. Nonwounded epidermis (hatched bars) was used as a control. Histogram represents average data from five regions surrounding a wound from *n* = 3 mice per condition. Error bars are SD. Statistical values were computed using a Student's *t* test. L) Images of explanted skin from control (IFT20 +/fl) and IFT20 cKO (IFT20 fl/fl) mice 14 days after explant. Tomato fluorescent (red) cells are HF-SCs which have migrated outward. Scale bar is 167 μm. Dotted line demarcates border of explant. Quantification of HF-SC migration in explants is provided on the right. Data is from *n* = 3 independent samples for each condition. * indicates *p* = 0.013 by Student's *t* test.

that the cilium could act as a mechanosensor that determines the direction of cell migration (Veland *et al.*, 2014). This could be particularly important in vivo, where changes in extracellular matrix deposition or altered topology must be sensed as cells invade and migrate in response to regenerative signaling. How ciliary functions/signaling integrate with the cell migration machinery is not well understood, and whether IFTs also function in a nonciliary context to regulate cell migration and invasion is an emerging area of investigation.

Data from this study indicate that Ift20 functions in an extraciliary role to drive cell migration by modulating FA dynamics and integrin trafficking. In contrast with previously reported results in fibroblasts (Christensen *et al.*, 2013), we find that the majority of wild-type cultured primary keratinocytes lack a primary cilium during directed migration (Supplemental Figure 2), suggesting that keratinocyte migration may not be hindered by loss of primary cilia to the extent of fibroblast migration. This difference in ciliation status may be a result of different cell types requiring different cues for cell migration.

compartments. Boxed regions are shown magnified in F). Scale bar indicates 10 μm. (F) Magnification of Rab5 endosomes and β1 integrin puncta. Arrows at 90 min point to colocalization of β1 integrin/Rab5 puncta in +Cre IFT20 fl/fl cKO cells. Scale bar indicates 5 μm. (E) The colocalization coefficient between Rab5 and β1 integrin was calculated at various time points of FA disassembly/MT regrowth (min indicates minutes); data in plot represents 60–81 cells from two independent experiments. *P* values calculated using Mann–Whitney U test.

Fibroblasts have been shown to depend on primary cilia to sense chemical cues such as platelet-derived growth factor AA (PDGF-AA) during cell migration, as their primary cilia are embedded with a variety of receptors including PDGF receptor alpha (PDGFRα) (Schneider et al., 2005; Clement et al., 2013; Umberger and Caspary, 2015). Interestingly, keratinocytes are a major source of cutaneous PDGF, especially during wound healing, but they themselves likely lack PDGF receptors (Ansel et al., 1993), suggesting a difference in migration cues between keratinocytes and fibroblasts. This difference in cues highlights possible differences in the extent by which primary cilia regulate migration between different cell types.

Interestingly, several studies have previously reported extraciliary functions for various IFT proteins in driving aspects of collective cell migration, in particular a role for Ift20 in nonciliated cancer cells (Nishita et al., 2017; Aoki et al., 2019). In these studies, it has been suggested that loss of Ift20 produces defects in the polarization of the Golgi apparatus or integrity of Golgi organization that are at the root of Ift20-dependent defects in cell motility. More specifically, loss of Ift20 can disrupt polarization of the Golgi complex and subsequent organization of Golgi-associated microtubules during cell migration (Aoki et al., 2019) or disrupt Golgi integrity and subsequent Golgi-dependent trafficking of a membrane receptor crucial for cancer cell invasion (Nishita et al., 2017).

In keratinocytes, we find that Golgi structure and integrity as well as Golgi polarity during migration are not significantly altered following loss of IFT20 (Supplemental Figure 1). Unlike cancer cells, in which the Golgi complex fragments subsequent to loss of IFT20 (Nishita et al., 2017), the Golgi complex of keratinocytes appears perinuclear and noncompact even in wild-type keratinocytes, and there is no significant increase in Golgi fragmentation in IFT20-null keratinocytes (Supplemental Figure 1, D and E). Furthermore, the polarity of the Golgi complex in keratinocytes is not significantly altered in IFT20-null keratinocytes compared with wild type during cell migration (Supplemental Figure 1, A–C). Taken together, these findings suggest that Golgi fragmentation and loss of Golgi polarity does not fully elucidate the migration defect we observe in keratinocytes following IFT20 ablation. These differences in Golgi compactness and structure between keratinocytes and cancer cells may be simply intrinsic differences between the cell types. Other studies have reported similar findings with regard to the perinuclear scattering and relative noncompactness of the Golgi complex in human keratinocytes (Madison and Howard, 1996; Behne et al., 2003).

Our data reveal a novel role for Ift20 in modulating mechanotransduction and FA turnover during keratinocyte migration. We find that IFT20 null keratinocytes demonstrate smaller and fewer FAs with reduced activation of FAK compared with wild-type controls. Using NZ treatment followed by washout to induce MT regrowth, we were able to interrogate the FA disassembly and reassembly processes during FA turnover. We find that FA reformation but not disassembly is impaired in IFT20 null keratinocytes. FA turnover (disassembly followed by reassembly of FAs) has previously been characterized to depend on MTs and the recycling of active integrins together with FAK and Src kinases through Rab5 and Rab11 endosomal compartments (Ezratty et al., 2005, 2009; Nader et al., 2016). Loss-of-function or dominant-negative mutations in Rab5 or Rab11 inhibit reassembly (reformation) but not disassembly of FAs (Nader et al., 2016). Src kinase inhibitors have also been found to inhibit reassembly but not disassembly of FAs (Nader et al., 2016).

In nonciliated T-cells, IFT20 has been reported to regulate polarized trafficking of cell surface receptors at the immune synapse (Finetti et al., 2009, 2014). This previous work demonstrated that Ift20 interacts with Rab5 and Rab11 to orchestrate the polarized recycling of surface T-cell receptors (TCRs) at the immune synapse (IS) (Finetti et al., 2019, 2020). Loss of IFT20 results in entrapment of TCRs in Rab5 endosomes (Finetti et al., 2014), similar to what we observe with β1 integrin during FA turnover. Likewise, the IS and FAs are also homologous in nature: both are formed via clustering of cell surface receptors at sites of cell adhesion, where accessory proteins and cytoskeletal components (such as actin) are recruited in response to mechanotransduction at the cell membrane. We postulate that Ift20 plays an analogous role in orchestrating the polarized recycling of an adhesion receptor (β1 integrin) in order to control assembly and mechanotransduction at FAs.

Consistent with this hypothesis, we find that loss of IFT20 reduces β1 integrin levels at FAs, a finding in line with the smaller and fewer FAs observed in these IFT20-null cells (Figure 2). Furthermore, our data suggest that like fibroblasts, keratinocyte FA turnover is dependent on recycling of integrins through a Rab5 early endosomal compartment and that Ift20 can colocalize at these compartments during this recycling process (Figure 6). Quantitative microscopy analyses showed that β1 integrin becomes entrapped in Rab5 (+) endosomes during FA turnover in IFT20-null keratinocytes (Figure 6). Surface labeling experiments demonstrated that IFT20-null keratinocytes do not show the expected significant increase in surface β1 integrin as compared with control during the FA reassembly process (Figure 4D). We conclude that IFT20 drives integrin trafficking through the early endosome en route to a recycling pathway required for subsequent integrin engagement into newly reforming FAs. Further investigation is warranted to determine whether integrins are recycled in an active conformation together with FAK and Src kinases during FA turnover (Nader et al., 2016) and what mechanistic role IFT20 might play in this process. To our knowledge this is the first study to specifically implicate IFT20 in integrin trafficking and signaling, although loss of primary cilia through KO of Kif3a has been previously shown to depress FAK phosphorylation—-a biochemical readout of integrin and adhesion-mediated mechanotransduction—-in chondrocytes during bone development (Song et al., 2007). FAK has recently been shown to regulate activation of the Rab5 GTPase cycle at early endosomes (Arriagada et al., 2019). It is interesting to speculate that IFT20 may orchestrate integrin transit from early endosomes via a FAK/Rab5 GTPase-dependent mechanism.

Consistent with our in vitro data, we observe both an in vivo and ex vivo migration defect when IFT20 is conditionally ablated in HF-SCs of the epidermis during wound healing. Wound healing is a complex process in which HF-SCs initiate repair of the wound by migrating toward the wound bed in an initial reepithelialization of the wound, after which epidermal cells derived from IFE complete the reepithelialization process (Ito et al., 2005; Ito and Cotsarelis, 2008). It has been suggested that this initial reepithelialization while not necessary for complete wound repair does accelerate wound healing (Langton et al., 2008). As such, further study into Ift20 and other cellular mechanisms that govern the HF-SC migratory response is necessary. The extracellular signals that mobilize stem cells have not been well-established (Gonzales and Fuchs, 2017) but may involve Wnt signaling through GSK3 and ACF7 (Wu et al., 2011) and genomic regulation by Sox9 and its downstream target genes (Nowak et al., 2008). Interestingly, IFT57, which interacts with IFT20, was identified as a bona fide HF-SC signature gene regulated by Sox9 (Kadaja et al., 2014). Further investigation into the ciliation status of these migrating HF-SCs in vivo and in explanted skin is warranted, but because we observe limited primary cilia in migrating cells in vivo (unpublished data), we speculate that these migration

defects in vivo may not be simply explained by loss of primary cilia. We propose, given our in vitro results, that the reduced migration and invasion observed in IFT20 cKO HF-SCs in vivo and in explanted skin results from defects in integrin recycling and mechanotransduction in the absence of an extraciliary Ift20 function.

Overall, we have demonstrated a novel role for Ift20 in regulating polarized cell migration and epidermal wound repair. Our data suggest that IFT20 regulates cell migration by governing FA turnover and integrin recycling in keratinocytes. These functions of Ift20 appear to be extraciliary and instead indicate a role for Ift20 in cellular mechanotransduction and cell motility through regulating surface integrin levels and FA dynamics. Ift20, and perhaps other ciliary or regulatory proteins, might be harnessed to promote stem cell migration in order to speed wound healing during tissue regeneration.

MATERIALS AND METHODS
Generation of mouse lines
All mice were housed and bred according to Columbia University IACUC approved protocols. K15-CrePR1 mice (Jackson Laboratory; Stock No. 005249) were bred with Ai9 mice (Jackson Laboratory; Stock No. 007909) to generate K15-Cre+; Rosa26-tdTomato fl/fl mice. These mice were then bred with Ift20 fl/fl mice (Jackson Laboratory; Stock No. 012565) to generate K15-Cre+; Ift20 fl/fl; Rosa26-tdTomato fl/fl mice. Genotyping was performed according to Jackson Laboratory recommendations using the following primer sets: Cre forward, 5'-GATATCTCACGTACTGACGG-3'; Cre reverse, 5'-TGAC-CAGAGTCATCCTTAGC-3'; Ift20 forward, 5'-ACTCAGTATGCAG-CCCAGGT-3'; Ift20 reverse, 5'-GCTAGATGCTGGGCGTAAAG-3'; TomatoWT forward, 5'-AAGGGAGCTGCAGTGGAGTA-3'; TomatoWT reverse, 5'-CCGAAAATCTGTGGGAAGTC-3'; TomatoMut forward, 5'-GGCATTAAAGCAGCGTATCC-3'; TomatoMut reverse, 5'-CTGTT-CCTGTACGGCATGG-3'.

In vivo ablation of Ift20 in HF-SCs and wound healing experiments
All surgical protocols were approved by the Columbia University IACUC. Mice were bred such that litters contained both K15Cre+; Ift20 fl/fl; Rosa26-tdTomato fl/fl (conditional knockout) and K15Cre+; Ift20 +/fl; Rosa26-tdTomato fl/fl (control) littermates. At postnatal day 21 or 22, the back skins of the mice was shaved and a topical solution of 1% RU486 (Mifepristone; Cayman Chemical 10006317) diluted in 70% ethanol was applied daily for 6–7 d. Between postnatal days 28 and 31, following the completion of RU486 treatment, the back skins of the mice were wounded with a full-thickness 6 mm punch biopsy. Four days following the wound, the mice were killed and the backskin was dissected away, vigorously washed in PBS, and either immediately frozen in O.C.T compound (Tissue-Tek 4583) or fixed in 4% paraformaldehyde (PFA) for 2–3 h and then vigorously washed in PBS prior to being frozen in O.C.T compound.

Isolation and culture of primary mouse keratinocytes
Primary mouse keratinocytes were isolated and cultured as previously described. Briefly, mouse pups between P0 and P4 were killed and their back skins removed and treated with Dispase (50 mg/ml; Life Technologies 17105041) for 2 h at 37°C or overnight at 4°C. The epidermal layer was peeled away from the dermal layer of the backskin. The epidermis was then floated in a 1:1 0.25% trypsin EDTA (Life Technologies)/Versene (Life Technologies 1504066) mixture and incubated at room temperature for 15 min, allowing for dissociation of the epidermal cells. Low-calcium E media was then added to the mixture and vigorously pipetted. The cell mixture was then filtered through 70 and 40-μm strainers, centrifuged at $1100 \times g$, and resuspended in low-calcium E media prior to being plated on Mitomycin C–treated 3T3 fibroblast monolayers. The keratinocytes were placed in a 37°C, 7.5% CO_2 incubator and continually passaged onto fresh Mitomycin C–treated 3T3 fibroblast monolayers as necessary. After 7 to 10 passages, the keratinocytes gained the ability to propagate without the fibroblasts. The keratinocytes were then continually cultured in low-calcium E media or frozen in low-calcium E media with 10% dimethyl sulfoxide.

Mitomycin C–treated 3T3 monolayers
3T3 fibroblasts were grown to confluency on 100 mm dishes in DMEM with 10% bovine calf serum at 37°C and 7.5% CO_2. The dishes were treated with Mitomycin C (8 μg/ml; Fisher BP25312) for 2 h at 37°C, after which the dishes were washed with phosphate-buffered saline (PBS) and given fresh media. Monolayers were maintained until ready for use up to 1 wk following Mitomycin C treatment.

Generation of lentivirus and transduction of keratinocytes
Lentiviral NLS-iCre-GFP was a gift from Elaine Fuchs (The Rockefeller University). Lentivirus was produced as previously described (Bhattarai et al., 2019). Briefly, the lentiviral plasmid was cotransfected with a pMD.2G envelope plasmid (Addgene #12259) and a psPAX2 packaging plasmid (Addgene #12260) using calcium phosphate/HBS into 293FT cells cultured in DMEM containing 10% fetal bovine serum (FBS) and G418/Geneticin. One day following transfection the media was replaced with Ultraculture Media (Lonza 12-725F) supplemented with 1% penicillin/streptomycin/L-glutamine, 1 mM sodium pyruvate, 0.075% sodium bicarbonate, and 5 mM sodium butyrate. Forty-eight hours after transfection, viral supernatant was collected from the cultures.

Transduction of keratinocyte cultures was performed as previously described (Bhattarai et al., 2019). Briefly, keratinocytes were grown to 70–80% confluency in a six-well plate. Immediately prior to viral transduction, 3 μl of Polybrene (10 mg/ml; Sigma Aldrich 107689) and 50–100 μl of viral supernatant were added per well. The plate was centrifuged at $1100 \times g$ at 37°C for 30 min, after which the media was replaced with fresh low-calcium E-media. Successful transduction was confirmed 2–3 d afterward.

In vitro migration assays and quantification
Cells were grown in two-well silicone inserts (Ibidi 80209) in 24-well plates until confluent. The insert was then removed to form a 500 μm defined cell-free gap. The cells were then washed with PBS and given fresh media. Cell migration was imaged using an IX-83 Olympus inverted microscope at 0 h and 18 h after start of migration. Migration rate was calculated as the area covered over time.

FA disassembly/reassembly assay
FA disassembly/reassembly assays were performed as previously described (Ezratty et al., 2005, 2009; Nader et al., 2016). Briefly, keratinocytes were grown on fibronectin-coated coverslips until confluent and then serum starved for 18–24 h in serum-free low calcium E media. The keratinocytes were then treated with 10 μM NZ (Sigma-Aldrich M1404) in serum free low calcium E media for 3–4 h, washed with PBS, and placed in fresh serum-free low calcium E media. At the desired time points, the cells were then either fixed for 10 min with 4% PFA for subsequent IF or scraped off the cell coverslip with a cell scraper and incubated with antibodies for subsequent flow cytometry.

IF of fixed cells

Following fixation, coverslips were washed with PBS and then permeabilized for 10 min with 0.3% TritonX in PBS. After being washed with PBS, coverslips were blocked for 1 h with 5% normal donkey serum (NDS), 5% normal goat serum (NGS), or a mix of 5% NGS/NDS in PBS at room temperature, after which they were incubated at 4°C overnight with the primary antibody diluted in the blocking buffer. Coverslips were then washed with PBS several times and then incubated at room temperature with appropriate secondary antibodies diluted in the blocking buffer for 1.5 h. After being washed several times with PBS, coverslips were mounted on slides with ProLong Gold Antifade Mountant with DAPI (4′,6-diamidino-2-phenylindole) (Invitrogen P36931). The following antibodies and dilutions were used: Ift20 (1:200; Proteintech 13615-1-AP), Arl13b (1:200; Proteintech 17711-1-AP), acetylated tubulin (1:1000; Sigma-Aldrich T7451), GM130 (1:200; BD 610822), vinculin (1:200; Sigma-Aldrich V4505), phospho-FAK Y397 (1:200; Invitrogen 44-624G), Rab5A (1:400; Cell Signaling Technology 46449T), CD29/beta1 integrin (1:100; Invitrogen 11-0291-82), donkey anti-rabbit Alexa Fluor 488 (1:500; Invitrogen A32790), donkey anti-rabbit Alexa Fluor 647 (1:500; Invitrogen A32795), donkey anti-mouse Alexa Fluor 488 (1:500; Invitrogen A32766), donkey anti-mouse Alexa Fluor 647 (1:500; Invitrogen A32787), and goat anti-Armenian hamster Alexa Fluor 488 (1:500; Jackson ImmunoResearch 127-545-160).

Collection of protein lysate

Cells were grown to confluency on glass coverslips. Cells were washed with ice-cold PBS, scraped off the coverslip, and lysed in ice-cold RIPA buffer with HALT protease and phosphatase inhibitors (Thermo Scientific 78440) for 30 min with regular agitation. Afterward the cell lysates were centrifuged, and the protein-rich supernatant was collected. The total protein concentration was quantified using a BradfordUltra assay (Expedeon BFU05L) according to the manufacturer's instructions.

Western blotting

Western blots were performed using a NuPAGE electrophoresis system (Invitrogen) according to the manufacturer's instructions. Briefly, 20–30 µg of total protein was loaded per lane into precast NuPAGE Novex Bis-Tris gels (Invitrogen NP0335BOX) and run in either MES SDS or MOPS SDS (Invitrogen NP0002, Invitrogen NP0001) running buffers. The gels were then transferred onto 0.2-µm-pore-size nitrocellulose membranes (Invitrogen LC2000) in NuPAGE transfer buffer (Invitrogen NP0006). Membranes were then blocked in a solution of TBS with 5% bovine serum albumin (BSA) for 1 h and then incubated overnight at 4°C with primary antibody diluted in TBS with 0.2% Tween-20 (2X TBST) and 5% BSA. Membranes were then washed with 0.1% Tween 20/TBS (1X TBST) and incubated for 1 h at room temperature with secondary antibodies diluted in 2X TBST with 5% BSA. After being washed with 1X TBST, the membrane was imaged using a LI-COR Odyssey Fc imaging system. The following antibodies and dilutions were used: phospho-FAK (1:1000; Invitrogen 44-624G), Ift20 (1:500; Proteintech 13615-1-AP), alpha-tubulin (1:1000; Sigma-Aldrich T9025), Rab5A (1:1000; Cell Signaling Technology 46449T), IRDye 800CW donkey anti-rabbit (1:10,000; Li-Cor 926-32213), and IRDye 680RD donkey anti-mouse (1:10,000; Li-Cor 926-68072).

Quantification of Western blots

Intensities of Western blot bands were quantified using the ImageJ Gel analysis function. Intensities were normalized to control bands for comparison between conditions.

Cell surface labeling of cultured keratinocytes

Labeling of cell surface integrin was performed as previously described (Ezratty et al., 2005, 2009; Nader et al., 2016). Briefly, cells were grown to confluency on glass coverslips. Cells were then scraped into ice-cold PBS and washed once with PBS. Approximately 1×10^5 cells per sample were incubated on ice with antibodies diluted in PCN (PBS with 0.5% bovine calf serum and 0.1% NaN_3) with Zombie Violet Dye (1:1000; BioLegend 423113) for 30 min. Samples were then washed once with PCN to remove unbound antibody and fixed in ice-cold 4% PFA diluted in PCN for 10 min. After washing samples with PCN to remove residual PFA, the samples were analyzed on a Bio-Rad ZE5 Cell Analyzer, and subsequent data were analyzed with FlowJo software. Antibodies and dilutions used are as follows: CD29 (integrin beta 1)-APC (1:10,000, 17-0291-82).

Cell surface labeling analysis

The average fluorescence intensity of integrin in Zombie Violet–low cells (i.e., live cells) was quantified using FlowJo. The same fluorescence intensity was quantified in nonstained cells to measure average background fluorescence. To normalize intensities, the average background fluorescence was subtracted from each of the average fluorescence intensity measurements from the various stained samples. These values were then normalized to the desired time point (i.e., 0 min during NZ washout).

Isolation of HF-SCs through flow cytometry

HF-SCs were isolated as previously described (Nowak and Fuchs, 2009) with minor adjustments. Briefly, mice were killed at appropriate time points and the backskins were shaved and removed. Using a blunted scalpel, the subcutaneous dermal fat of each backskin was scraped away in a dish of cold HBSS. For telogen skin, the backskin was then directly incubated with 0.25% trypsin EDTA (Life Technologies) at 37°C for 1 h with the epidermis facing upward. For anagen skin, the backskin was first incubated with 0.25% (wt/vol) type I collagenase in HBSS for 40 min at 37°C, after which the dermis was scraped away with a blunted scalpel prior to floating the backskin epidermis upward in 0.25% trypsin EDTA (Life Technologies) and incubated for 30 min at 37°C. After adding cold D10 (DMEM with 10% FBS) to neutralize the trypsin, the HFs were scraped into the D10/trypsin mixture using a blunted scalpel, and any remaining dermis was removed. The HF/D10/trypsin mixture was then vigorously pipetted to break up clumps and then transferred into a bottle with a stir bar. After the mixture was stirred for at 4°C for 30 min, the mixture was strained through a 70-µm filter and then a 40-µm filter. The HF-SCs were then centrifuged at 1100 × g and washed once with cold D10. At this point ~5% of the cells can be separated and used to prepare compensation staining samples if necessary. The remaining cells were then stained with CD34-eFluor660 (1:75; Invitrogen 50-0341-82) and CD49f (integrin alpha 6)-FITC (Fluorescein Isothiocyanate) (1:100; Invitrogen 11-0495-82) in D10 on ice for 30–45 min with intermittent agitation of the samples. The samples were then centrifuged at 1100 × g and washed once with D10 media. The samples were then centrifuged again and then resuspended in D10 media with DAPI (1:1000; Invitrogen D1306). Cells were then sorted on a BD FACS Aria II cell sorter. Live HF-SCs were gated as being DAPI-low, CD34-high, CD49f-high, and tdTomato-high cells and sorted into TRIzol LS (Invitrogen; 10296028) and sorted into TRIzol LS (Invitrogen; 10296028).

qPCR of HF-SCs

RNA was extracted in TRIzol LS (Invitrogen; 10296028) per the manufacturer's instructions. cDNA was generated from the RNA

using the Verso cDNA Synthesis Kit (Thermo Scientific; AB1453B) per the manufacturer's instructions using all RNA. qPCR for each cDNA sample was performed in triplicate using Thermo Scientific Maxima SYBR Green/ROX qPCR Master Mix (2x) (Thermo Scientific; K0221). The primers used for qPCR were as follows: Ift20 forward, 5'-TCCTGATTGCCACTGTCACC-3' and Ift20 reverse, 5'-GTCCAACACTCGGAGCTTGT-3'.

IF of tissue sections

Tissues embedded in O.C.T compound were sectioned using a Cryostat (Leica) at 10-µm thin sections onto glass slides. The sections were then stained according to previously described protocols (Bhattarai *et al.*, 2019). Briefly, unfixed sections were first fixed for 10 min in 4% PFA at room temperature. Sections were then blocked in gelatin blocking solution (2.5% normal donkey serum, 2.5% normal goat serum, 1% BSA, 2% fish gelatin, and 0.3% Triton-X in PBS) for 1–2 h at room temperature. Sections were then incubated overnight at 4°C with the primary antibodies diluted in gelatin blocking solution. After being washed several times with PBS to remove residual unbound antibody, sections were incubated for 1–2 h at room temperature in secondary antibodies diluted in gelatin blocking solution. After being washed with PBS, the sections were mounted with coverslips using ProLong Gold Antifade Mountant with DAPI (Invitrogen P36931). The following antibodies and dilutions were used: Ift20 (1:200; Proteintech 13615-1-AP), Arl13b (1:200; Proteintech 17711-1-AP), acetylated tubulin (1:1000; Sigma-Aldrich T7451), GM130 (1:200; BD 610822), donkey anti-rabbit Alexa Fluor 488 (1:500; Invitrogen A32790), donkey anti-rabbit Alexa Fluor 647 (1:500; Invitrogen A32795), donkey anti-mouse Alexa Fluor 488 (1:500; Invitrogen A32766), and donkey anti-mouse Alexa Fluor 647 (1:500; Invitrogen A32787).

Explant biopsy culture and quantification

The biopsy samples from the wounded mice were collected and plated on fibronectin-coated tissue culture dishes and covered in low-calcium E-media. Culture media was replaced every 4–5 d. After 14 d of culturing, NucBlue Live Cell Stain (Invitrogen R37605) was added to the culture media to label nuclei and the sample was imaged using a fluorescence microscope. Migration of tdTomato-positive hair follicle stem cells was quantified by calculating the number of tdTomato-positive cells that had migrated out of the tissue sample per circumferential length of the tissue sample (number of tdTomato-positive cells/circumference of biopsy).

Image acquisition

Confocal images were acquired with an Olympus IX83 DSU unit with Hamamatsu Orca-r2 through 63x (N.A 1.4) oil or 4x (N.A. 0.10) Plan-Apochromat objectives and equipped with the following Chroma filter sets: 49008 ET TR C94094 (mRFP1), 49004 ET dsR C94093 (Cy3, DyLight549), 41008 Cy5 (Cy5), 41001 FITC (Alexa-Fluor 488/GFP). For images of tissue sections, Z-stacks of 5–15 planes (0.5 µm) were captured, and either representative single Z-planes or maximum projections (three images) are presented. For images of in vitro cells, Z stacks of 3–5 planes (0.5 µm) were captured and representative single Z planes are shown. Image acquisition was driven using Metamorph (Olympus). Image processing was performed using ImageJ.

FA and colocalization image quantification

Image quantification was performed using ImageJ. Briefly, the background of images was first subtracted using the rolling ball radius background subtraction function in ImageJ. Individual cells were identified and saved as regions of interest (ROIs). Images were then converted to 8-bit images and thresholded according to the structures of interest (i.e., FAs, endosomes, etc.). Using the analyze particles function in ImageJ, the structures of interest within each ROI were quantified by number and area. Average total area of FAs per cell and average FA area were computed based on these data. Co-localization coefficients between Rab5A and Ift20 or Rab5A and β1 integrin in cells were computed using the size-based colocalization coefficient defined in Rizk *et al.* (2015) (area of Ift20 that colocalizes with Rab5A/total area of Ift20 or area of beta 1 integrin that colocalizes with Rab5A/total area of beta 1 integrin).

Statistics

All statistical analysis was performed using Mann–Whitney U tests or Student's *t* tests using R statistical software. The test performed for each set of data is indicated in the figure legends.

REFERENCES

Absalon S, Blisnick T, Kohl L, Toutirais G, Dore G, Julkowska D, Tavenet A, Bastin P (2008). Intraflagellar transport and functional analysis of genes required for flagellum formation in trypanosomes. Mol Biol Cell 19, 929–944.

Ansel JC, Tiesman JP, Olerud JE, Krueger JG, Krane JF, Tara DC, Shipley GD, Gilbertson D, Usui ML, Hart CE (1993). Human keratinocytes are a major source of cutaneous platelet-derived growth factor. J Clin Invest 92, 671–678.

Aoki T, Nishita M, Sonoda J, Ikeda T, Kakeji Y, Minami Y (2019). Intraflagellar transport 20 promotes collective cancer cell invasion by regulating polarized organization of Golgi-associated microtubules. Cancer Sci 110, 1306–1316.

Arriagada C, Silva P, Millet M, Solano L, Moraga C, Torres VA (2019). Focal adhesion kinase-dependent activation of the early endocytic protein Rab5 is associated with cell migration. J Biol Chem 294, 12836–12845.

Behne MJ, Tu CL, Aronchik I, Epstein E, Bench G, Bikle DD, Pozzan T, Mauro TM (2003). Human keratinocyte ATP2C1 localizes to the Golgi and controls Golgi Ca2+ stores. J Invest Dermatol 121, 688–694.

Bhattarai SR, Begum S, Popow R, Ezratty EJ (2019). The ciliary GTPase Arl3 maintains tissue architecture by directing planar spindle orientation during epidermal morphogenesis. Development 146, dev161885.

Bose A, Teh MT, Mackenzie IC, Waseem A (2013). Keratin k15 as a biomarker of epidermal stem cells. Int J Mol Sci 14, 19385–19398.

Burridge K (2017). Focal adhesions: a personal perspective on a half century of progress. FEBS J 284, 3355–3361.

Chen KE, Healy MD, Collins BM (2019). Towards a molecular understanding of endosomal trafficking by Retromer and Retriever. Traffic 20, 465–478.

Christensen ST, Veland IR, Schwab A, Cammer M, Satir P (2013). Analysis of primary cilia in directional cell migration in fibroblasts. Methods Enzymol 525, 45–58.

Clement DL, Mally S, Stock C, Lethan M, Satir P, Schwab A, Pedersen SF, Christensen ST (2013). PDGFRalpha signaling in the primary cilium regulates NHE1-dependent fibroblast migration via coordinated differential activity of MEK1/2-ERK1/2-p90RSK and AKT signaling pathways. J Cell Sci 126, 953–965.

Ezratty EJ, Bertaux C, Marcantonio EE, Gundersen GG (2009). Clathrin mediates integrin endocytosis for focal adhesion disassembly in migrating cells. J Cell Biol 187, 733–747.

Ezratty EJ, Partridge MA, Gundersen GG (2005). Microtubule-induced focal adhesion disassembly is mediated by dynamin and focal adhesion kinase. Nat Cell Biol 7, 581–590.

Ezratty EJ, Stokes N, Chai S, Shah AS, Williams SE, Fuchs E (2011). A role for the primary cilium in Notch signaling and epidermal differentiation during skin development. Cell 145, 1129–1141.

Finetti F, Capitani N, Baldari CT (2019). Emerging roles of the intraflagellar transport system in the orchestration of cellular degradation pathways. Front Cell Dev Biol 7, 292.

Finetti F, Cassioli C, Cianfanelli V, Onnis A, Paccagnini E, Kabanova A, Baldari CT (2020). The intraflagellar transport protein IFT20 controls lysosome biogenesis by regulating the post-Golgi transport of acid hydrolases. Cell Death Differ 27, 310–328.

Finetti F, Paccani SR, Riparbelli MG, Giacomello E, Perinetti G, Pazour GJ, Rosenbaum JL, Baldari CT (2009). Intraflagellar transport is required for polarized recycling of the TCR/CD3 complex to the immune synapse. Nat Cell Biol 11, 1332–1339.

Finetti F, Patrussi L, Masi G, Onnis A, Galgano D, Lucherini OM, Pazour GJ, Baldari CT (2014). Specific recycling receptors are targeted to the immune synapse by the intraflagellar transport system. J Cell Sci 127, 1924–1937.

Follit JA, Tuft RA, Fogarty KE, Pazour GJ (2006). The intraflagellar transport protein IFT20 is associated with the Golgi complex and is required for cilia assembly. Mol Biol Cell 17, 3781–3792.

Fuchs E (2016). Epithelial skin biology: three decades of developmental biology, a hundred questions answered and a thousand new ones to address. Curr Top Dev Biol 116, 357–374.

Galgano D, Onnis A, Pappalardo E, Galvagni F, Acuto O, Baldari CT (2017). The T cell IFT20 interactome reveals new players in immune synapse assembly. J Cell Sci 130, 1110–1121.

Goetz SC, Anderson KV (2010). The primary cilium: a signalling centre during vertebrate development. Nat Rev Genet 11, 331–344.

Gonzales KAU, Fuchs E (2017). Skin and its regenerative powers: an alliance between stem cells and their niche. Dev Cell 43, 387–401.

Ito M, Cotsarelis G (2008). Is the hair follicle necessary for normal wound healing? J Invest Dermatol 128, 1059–1061.

Ito M, Liu Y, Yang Z, Nguyen J, Liang F, Morris RJ, Cotsarelis G (2005). Stem cells in the hair follicle bulge contribute to wound repair but not to homeostasis of the epidermis. Nat Med 11, 1351–1354.

Jonassen JA, San Agustin J, Follit JA, Pazour GJ (2008). Deletion of IFT20 in the mouse kidney causes misorientation of the mitotic spindle and cystic kidney disease. J Cell Biol 183, 377–384.

Kadaja M, Keyes BE, Lin M, Pasolli HA, Genander M, Polak L, Stokes N, Zheng D, Fuchs E (2014). SOX9: a stem cell transcriptional regulator of secreted niche signaling factors. Genes Dev 28, 328–341.

Krylyshkina O, Kaverina I, Kranewitter W, Steffen W, Alonso MC, Cross RA, Small JV (2002). Modulation of substrate adhesion dynamics via microtubule targeting requires kinesin-1. J Cell Biol 156, 349–359.

Langton AK, Herrick SE, Headon DJ (2008). An extended epidermal response heals cutaneous wounds in the absence of a hair follicle stem cell contribution. J Invest Dermatol 128, 1311–1318.

Madison KC, Howard EJ (1996). Ceramides are transported through the Golgi apparatus in human keratinocytes in vitro. J Invest Dermatol 106, 1030–1035.

Mayor R, Etienne-Manneville S (2016). The front and rear of collective cell migration. Nat Rev Mol Cell Biol 17, 97–109.

Nader GP, Ezratty EJ, Gundersen GG (2016). FAK, talin and PIPKIgamma regulate endocytosed integrin activation to polarize focal adhesion assembly. Nat Cell Biol 18, 491–503.

Nishita M, Park SY, Nishio T, Kamizaki K, Wang Z, Tamada K, Takumi T, Hashimoto R, Otani H, Pazour GJ, et al. (2017). Ror2 signaling regulates Golgi structure and transport through IFT20 for tumor invasiveness. Sci Rep 7, 1.

Nowak JA, Fuchs E (2009). Isolation and culture of epithelial stem cells. Methods Mol Biol 482, 215–232.

Nowak JA, Polak L, Pasolli HA, Fuchs E (2008). Hair follicle stem cells are specified and function in early skin morphogenesis. Cell Stem Cell 3, 33–43.

Rizk A, Mansouri M, Ballmer-Hofer K, Berger P (2015). Subcellular object quantification with Squassh3C and SquasshAnalyst. Biotechniques 59, 309–312.

Schneider L, Cammer M, Lehman J, Nielsen SK, Guerra CF, Veland IR, Stock C, Hoffmann EK, Yoder BK, Schwab A, et al. (2010). Directional cell migration and chemotaxis in wound healing response to PDGF-AA are coordinated by the primary cilium in fibroblasts. Cell Physiol Biochem 25, 279–292.

Schneider L, Clement CA, Teilmann SC, Pazour GJ, Hoffmann EK, Satir P, Christensen ST (2005). PDGFRalphaalpha signaling is regulated through the primary cilium in fibroblasts. Curr Biol 15, 1861–1866.

Singla V, Reiter JF (2006). The primary cilium as the cell's antenna: signaling at a sensory organelle. Science 313, 629–633.

Song B, Haycraft CJ, Seo HS, Yoder BK, Serra R (2007). Development of the post-natal growth plate requires intraflagellar transport proteins. Dev Biol 305, 202–216.

Spasic M, Jacobs CR (2017). Primary cilia: cell and molecular mechano-sensors directing whole tissue function. Semin Cell Dev Biol 71, 42–52.

Tapial Martinez P, Navajas PL, Lietha D (2020). FAK structure and regulation by membrane interactions and force in focal adhesions. Biomolecules 10, 179.

Tobin JL, Di Franco M, Eichers E, May-Simera H, Garcia M, Yan J, Quinlan R, Justice MJ, Hennekam RC, Briscoe J, et al. (2008). Inhibition of neural crest migration underlies craniofacial dysmorphology and Hirschsprung's disease in Bardet-Biedl syndrome. Proc Natl Acad Sci USA 105, 6714–6719.

Umberger NL, Caspary T (2015). Ciliary transport regulates PDGF-AA/alphaalpha signaling via elevated mammalian target of rapamycin signaling and diminished PP2A activity. Mol Biol Cell 26, 350–358.

Veland IR, Lindbaek L, Christensen ST (2014). Linking the primary cilium to cell migration in tissue repair and brain development. Bioscience 64, 1115–1125.

Waters AM, Beales PL (2011). Ciliopathies: an expanding disease spectrum. Pediatr Nephrol 26, 1039–1056.

Wu X, Shen QT, Oristian DS, Lu CP, Zheng Q, Wang HW, Fuchs E (2011). Skin stem cells orchestrate directional migration by regulating microtubule-ACF7 connections through GSK3beta. Cell 144, 341–352.

Zhao X, Guan JL (2011). Focal adhesion kinase and its signaling pathways in cell migration and angiogenesis. Adv Drug Deliv Rev 63, 610–615.